Electronic channels for acoustic transport in semiconductor heterostructures

K. Biermann,[a] O. D. D. Couto, Jr.,[b] W. Seidel, R. Hey, and P. V. Santos
Paul-Drude-Institut für Festkörperelektronik, Hausvogteiplatz 5-7, D-10117 Berlin, Germany

(Received 12 February 2010; accepted 2 April 2010; published online 21 April 2010)

We demonstrate electronic waveguides for the ambipolar transport of electrons and holes by surface acoustic waves (SAWs) in buried (Al,Ga)As quantum well (QW) structures, which do not require deep-etching for their fabrication. They are defined by tailoring the SAW-induced piezoelectric potential in the QW plane using thin metal stripes deposited onto the piezoelectric cap layer of the QW sample. Acoustic transport experiments show the enhanced capture and acoustic transport of photoexcited carriers underneath the metallic surface stripes. © *2010 American Institute of Physics*. [doi:10.1063/1.3407672]

A surface acoustic wave (SAW) propagating on a piezoelectric semiconductor (such as, for instance, GaAs) produces a moving piezoelectric potential Φ_{SAW}, which traps electrons and holes and transports them with the acoustic velocity v_{SAW}.[1] Acoustic transport has also been demonstrated for other electronic excitations including spins,[2] and excitons.[3] Due to the slow acoustic velocity as compared to the electronic ones, the carriers tend to diffuse laterally (i.e., along the SAW wavefronts) during the transport, leading to an effective channel width comparable to the width of the SAW beam. Many applications require narrow electronic channels—one example is the transfer of charge between a quantum well (QW) and a quantum wire or dot.[4] In the case of unipolar transport (i.e., where the SAW transports either electrons or holes), narrow channels can be defined by etching[5] or by biased metal gates.[6] These channels, however, are not compatible with the simultaneous transport of electrons and holes. In particular, etching normally creates trapping states that capture carriers of one polarity and induce recombination with carriers with the opposite polarity, thereby increasing the transport losses.

In this paper, we demonstrate a simple process for the fabrication of narrow ambipolar transport channels for acoustic transport within a buried QW based on the deposition of thin metal layers on the sample surface. These thin layers modify the depth distribution of the SAW piezoelectric field. In particular, the SAW piezoelectric potential in the plane of a buried QW can be made stronger underneath metal-covered surface areas, thus laterally confining the carriers. The confinement effects on the carriers is thus the electric analog to the index-guiding of light waves in a semiconductor laser structure, where the lateral change in the effective refractive index is accomplished by modifying only the uppermost cladding layers.[7] This concept does not require etching and can be applied to different material systems.

The feasibility of the concept is demonstrated by acoustic transport experiments carried out on a 20 nm thick undoped single GaAs QW embedded in a 2λ thick asymmetric microcavity with distributed Bragg reflectors (DBRs). The optical microcavity has been designed to match the QW emission wavelength at $T=20$ K. The structure was grown on a semi-insulating (SI) GaAs(110) substrate by molecular beam epitaxy.[8] Figure 1 shows a cross-section scanning electron micrograph of the microcavity. The position of the QW is indicated by the arrow. The lower (upper) DBR of this sample consists of 15.5 (4) pairs of $Al_{0.60}Ga_{0.40}As$ (dark regions)/$Al_{0.07}Ga_{0.93}As$ (bright regions) quarter-wavelength layers. In the lower DBR, every third $Al_{0.07}Ga_{0.93}As$ quarter-wavelength layer was replaced by a $3/4\lambda$ thick layer. The replacement does not affect the central stop-band wavelength of the DBR but helps to reduce the overall Al content of the epitaxial layers. Since the acoustic velocity of $Al_xGa_{1-x}As$ alloys increases with x, a low average Al content is essential to ensure the existence of propagating surface acoustic modes.

In order to increase the SAW generation efficiency, the samples were coated with a 420 nm thick ZnO piezoelectric layer deposited by sputtering. By taking this layer into account, the distance from the QW to the sample surface amounts to 1040 nm. Rayleigh SAWs propagating along the y [001] crystal direction (with frequency (f_{SAW}) and wavelength (λ_{SAW}) of 526 MHz and 5.6 μm, respectively) were generated by linear split-finger interdigital transducers (IDTs) deposited on the surface of the sample.

Piezoelectric carrier transport guides were produced by simply evaporating thin metal stripes on the surface of a ZnO

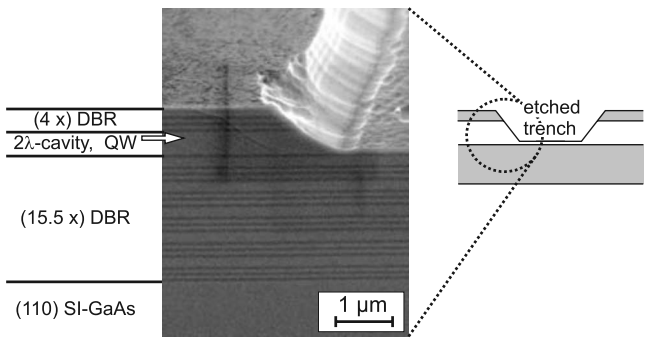

FIG. 1. Cross-sectional scanning electron micrograph of an (Al,Ga)As asymmetric cavity structure. The top ZnO layer was removed. The upper right side shows a trench formed by chemically etching the upper DBR and the cavity layers. The arrow indicates the position of the QW.

[a]Electronic mail: biermann@pdi-berlin.de.
[b]Present address: Hounsfield Road S3 7RH, University of Sheffield, Sheffield, United Kingdom.

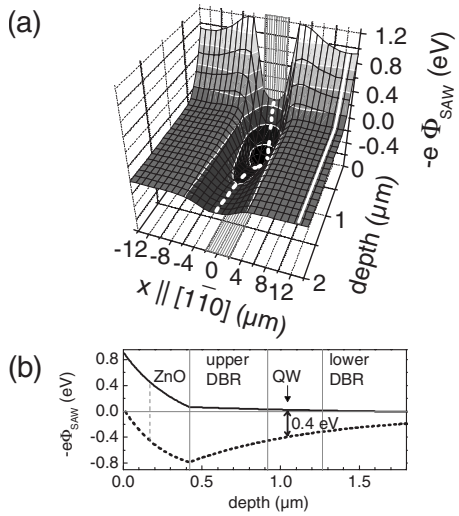

FIG. 2. (a) Gray scale plot of the piezoelectric energy $-e\Phi_{SAW}$ in the x-z plane. The shaded areas mark the x position of a 4 μm wide metallic surface stripe. The dashed and full white lines at x=0 μm (underneath the metallic stripe) and x=12.5 μm (underneath uncovered surface), respectively, indicate the depth profiles shown explicitly in (b). The phase of the acoustic wave was chosen to minimize the piezoelectric energy underneath the metallic stripe at the QW depth.

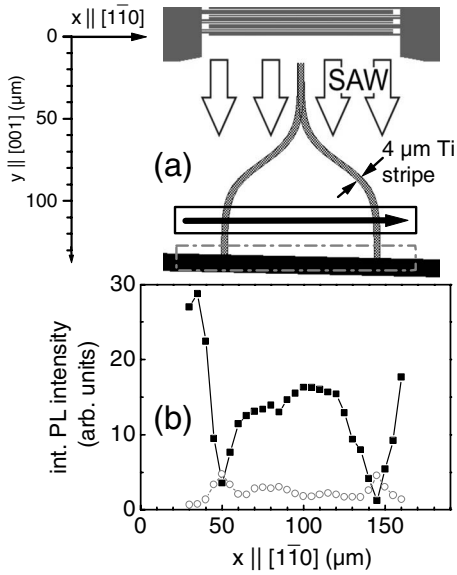

FIG. 3. (a) Schematic top view on the sample surface, depicting the linear IDT at the top and the Y-shaped metallic stripe defining the carrier waveguide. The horizontal arrow marks the scanning pathway of the laser beam. The black rectangle shows the trench used to block the transport and induce carrier recombination. The area for the generation (recombination) of the PL signal is bordered by the full (broken) line. (b) PL intensity integrated over the solid rectangle around the generation region (full squares) and over the dashed rectangle close to the recombination area (open circles) as a function of the excitation position.

layer deposited on the (Al,Ga)As sample. The metallic layer screens the dynamic electric field carried by the SAW at the sample surface. The effects of metallic surface stripes on the depth (z [110]) dependence of the piezoelectric energy $-e\Phi^0_{SAW}(z)$, where $\Phi_{SAW}(y,z,t)=\Phi^0_{SAW}(z)\cos 2\pi(y/\lambda_{SAW}-f_{SAW}t)$ describes the spatial dependence of the piezoelectric potential, was calculated using an elastic continuum model for the SAW fields.[9] Thereby, the lateral structure is assumed to be periodic, such that the two-dimensional problem can be solved by using a Fourier transformation. For the calculations the sample structure was approximated as a three-layer-system consisting of the ZnO cap layer, an averaged 3.4 μm thick $Al_{0.27}Ga_{0.73}As$ layer representing the (Al,Ga)As microcavity layers and the GaAs(110) substrate. Figure 2(a) shows the piezoelectric energy $-e\Phi_{SAW}$ in the x [1$\bar{1}$0]-z [110] plane. The shaded areas mark the lateral position of the 4 μm wide metallic surface stripe deposited on the surface. The dashed and full white lines at x=0 μm (underneath the metallic stripe) and x=12.5 μm (underneath uncovered surface), respectively, indicate the depth profiles shown explicitly in Fig. 2(b). As expected, $|\Phi_{SAW}|$ reaches its maximum at the free sample surface and vanishes directly underneath the metallic layer. The short-circuit of the piezoelectric potential caused by thin metal layers has been used to stop the transport and force the recombination of electrons and holes during acoustic transport in near-surface QWs.[1] The situation reverses away from the surface, where at the depth of $z=170$ nm [dashed vertical line in Fig. 2(b)] the modulus of the piezoelectric potential $|\Phi_{SAW}|$ becomes stronger underneath the metal. Thus, if a QW is placed deeper than at this cross-over depth, the stronger piezoelectric potential will then attract both electrons and holes, thereby forming a transport channel underneath the metal stripe. Assuming a linear acoustic power density of 40 W/m, the laterally confining energy is calculated to be on the order of 0.4 eV.

Carrier guiding during acoustic transport was investigated by spatially resolved photoluminescence (PL) at 20 K using the microcavity sample with a Y-shaped guiding titanium stripe, as illustrated in Fig. 3(a). The stripe is 7 nm thick and 4 μm wide. The carriers were excited within a 4 μm spot using a cw Ti:sapphire laser (wavelength and power are 797 nm and 3.9 μW, respectively). The PL along the transport path was collected by a microscopic objective and detected with spatial resolution of approximately 2 μm. In order to stop the transport, a trench was etched in the region indicated by the horizontal black stripe to weaken the SAW and force the recombination of the transported carriers—a cross-section view of the trench is shown in Fig. 1.

The solid and open symbols in Fig. 3(b) display intensity profiles of the PL emitted close to the generation spot (solid squares) and to the trench (open circles) recorded while scanning the excitation spot along the horizontal arrow indicated in Fig. 3(a). For each position of the laser spot, we have monitored the PL intensity integrated over the solid and dashed rectangles, respectively. The calculations predict a stronger piezoelectric field, and, therefore, higher carrier separation and transport efficiencies underneath the stripes. In agreement with this expectation, the PL near the generation point reduces when carriers are generated close to the stripes. This reduction is much larger than the one expected from the reduced transmissivity through the semitransparent Ti layer and stems from efficient transport of carriers away from the generation area. At the same time, the PL increases close to the trench (open symbols), thus indicating that more carriers reach this point. Unfortunately, due to the formation of nonradiative recombination centers at the etched sidewall, carriers arriving at the etched trench are more likely to recombine nonradiatively than radiatively. This explains why the reduction in the PL signal in the generation area exceeds by far the enhancement in the recombination area. Further-

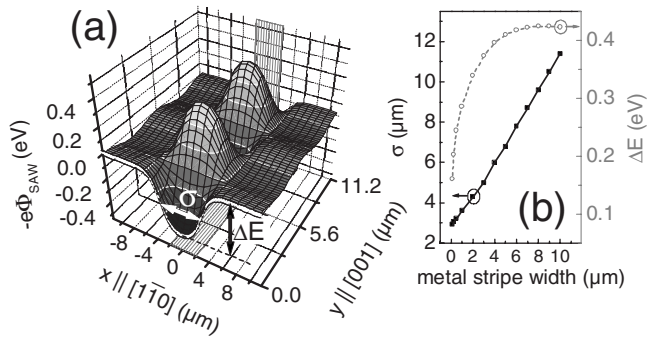

FIG. 4. (a) Two-dimensional plot of the piezoelectric energy $-e\Phi_{SAW}$ induced by a 5.6 μm SAW in the QW plane. The shaded areas mark the position of a 4 μm wide metallic surface stripe. σ and ΔE denote the FWHM and the energy barrier of the dynamic lateral confinement, respectively. (b) σ (black full squares) and ΔE (gray open circles) as a function of the width of a surface metallic stripe, calculated for a linear acoustic power density of 40 W/m.

more, we also observed that carriers reaching the etched trench diffuse along it before recombining. For this reason, in order to show the transport we have integrated the PL signals over rather extended areas. Note that the stripes in Fig. 3(a) are placed close to the borders of the acoustic beam. An enhanced transport underneath the stripe takes place despite the lower acoustic intensity as compared to the center of the SAW beam.

The most important properties of these lateral transport channels are given by the effective width [full width at half maximum (FWHM) σ] and the height (ΔE) of the confining potential at the position of the buried QW [as shown in Fig. 4(a)]. As expected, both σ and ΔE decrease with the width of the metallic surface stripes. These characteristics determine the feasibility of these channels for the intended applications and were therefore numerically analyzed. The gray scale plot in Fig. 4(a) illustrates a snapshot of the dynamic piezoelectric energy $-e\Phi_{SAW}$ in the QW plane induced by a 5.6 μm SAW. The shaded areas mark the position of a 4 μm wide metallic surface stripe. The surface metallic stripe affects the confining potential at the QW depth, as it is illustrated in Fig. 4(b) by plotting the width σ (black full squares) and the confining energy ΔE (gray open circles) as a function of the stripe width. The effective channel width scales linearly with the surface stripe width. Furthermore, the confining energy ΔE only reduces for very narrow stripes (<1 μm). Thus, for the investigated sample structure, a 2 μm wide metallic stripe would induce an effective channel width of only 4 μm while still preserving a considerable ΔE of 0.34 eV. It should be noted, that this expected effective channel width is smaller than the acoustic wavelength of $\lambda_{SAW}=5.6$ μm.

In conclusion, we have experimentally demonstrated that piezoelectric channels for the acoustic transport of electrons and holes can be created in a buried QW by placing metal stripes on the sample surface. As verified by two-dimensional calculations of the SAW fields, the metal stripes change the boundary conditions for the SAW piezoelectric potential at the surface, thereby leading to an enhancement of this potential in the QW regions underneath them.

We thank A.-K. Bluhm and U. Jahn for SEM investigations and B. Drescher for the ZnO coating. We also acknowledge gratefully the support from the Deutsche Forschungsgemeinschaft (priority Program No. SPP1285).

[1]C. Rocke, S. Zimmermann, A. Wixforth, J. P. Kotthaus, G. Böhm, and G. Weimann, Phys. Rev. Lett. **78**, 4099 (1997).
[2]T. Sogawa, P. V. Santos, S. K. Zhang, S. Eshlaghi, A. D. Wieck, and K. H. Ploog, Phys. Rev. Lett. **87**, 276601 (2001).
[3]J. Rudolph, R. Hey, and P. V. Santos, Phys. Rev. Lett. **99**, 047602 (2007).
[4]C. Wiele, F. Haake, C. Rocke, and A. Wixforth, Phys. Rev. A **58**, R2680 (1998).
[5]V. I. Talyanskii, V. Kachkanov, and P. V. Santos, Semicond. Sci. Technol. **23**, 125017 (2008).
[6]J. M. Shilton, V. I. Talyanskii, M. Pepper, D. A. Ritchie, J. E. F. Frost, C. J. B. Ford, C. G. Smith, and G. A. C. Jones, J. Phys.: Condens. Matter **8**, L531 (1996).
[7]I. Kaminow, L. Stulz, J. S. Ko, A. Dentai, R. Nahory, J. DeWinter, and R. Hartman, IEEE J. Quantum Electron. **19**, 1312 (1983).
[8]R. Hey, U. Jahn, Q. Wan, and A. Trampert, Phys. Status Solidi C **5**, 2917 (2008).
[9]M. M. de Lima, Jr., and P. V. Santos, Rep. Prog. Phys. **68**, 1639 (2005).